Misalignment Sensitivity of Strongly Coupled Wireless Power Transfer Systems

Daerhan Liu, *Student Member, IEEE*, Hao Hu, *Student Member, IEEE*, and Stavros V. Georgakopoulos, *Senior Member, IEEE*

***Abstract*—A traditional strongly coupled magnetic resonance (SCMR) system is highly sensitive to the alignment between the transmitter and receiver elements, which is an issue that has limited their applicability in practical wireless power transfer systems. This paper proposes, for the first time, a novel set of SCMR-based topologies that are less sensitive to misalignment while providing large wireless powering efficiencies. Specifically, instead of using planar coils for the transmitter and the receiver, we connect two orthogonal coils together into a 3-D model to provide misalignment insensitivity. Three SCMR systems (standard SCMR, conformal SCMR, and hybrid SCMR systems) are studied and compared to the proposed 3-D SCMR system in terms of angular azimuth, angular elevation, and lateral misalignment. Also, the ranges of these SCMR systems are compared. It is shown that the proposed misalignment system achieves above 40% efficiency for the entire range of 360° of angular misalignment. Also, our results show that the proposed misalignment system provides longer range.**

***Index Terms*—Efficiency, misalignment, strongly coupled magnetic resonance (SCMR), wireless power transfer (WPT).**

I. Introduction

WIRELESS power transfer (WPT) methods have been extensively utilized. Specifically, near-field WPT methods have been implemented in several applications, such as electric vehicles [1], radio-frequency identification [2], [3], implanted medical devices [4], and mobile devices [5]. Also, the strongly coupled magnetic resonance (SCMR) method is a WPT method that has been recently developed, and it provides larger efficiency at longer range than traditional near-field techniques [6]–[8]. In order for SCMR to achieve high efficiency, it requires that the transmitting (TX) and receiving (RX) elements (typically loops or coils) are designed so that they resonate at the frequency where the elements naturally exhibit maximum Q-factor [9]. The optimization of SCMR's efficiency has been examined by various papers. For example, an automated impedance matching system that matches the resonance frequency of the resonator pair to that of the power source was proposed in [10]. Also, SCMR's efficiency was improved by using a transmitter and a receiver that consists of two strongly coupled resonators in [11].

A disadvantage of conventional SCMR systems is that they are highly sensitive to the alignment between transmitter and receiver. An optimization technique for improving the efficiency of SCMR systems under lateral misalignment was presented in [12]. Specifically, 48.4% efficiency was achieved by using an adaptive matching network. However, no solution for angular misalignment was proposed in [12]. Also, the effects of few misalignment angles on SCMR's efficiency were examined in [13] and [14]. However, the main focus of [13] and [14] was to study multiple transmitter/receiver WPT systems and their misalignment analysis was very limited. Analytical formulations for the power transfer efficiencies of inductive links under lateral and angular coil misalignment were presented in [15]. In addition, the effects of angular and lateral misalignment in inductively coupled systems, which simultaneously achieve WPT and data communication, were examined in [16]. Also, the conformal SCMR (CSCMR) method, which has a source loop that is concentric and coplanar with the TX resonator (as well as a load loop that is concentric and coplanar with the RX resonator), was studied in [16]. Therefore, CSCMR systems are easier to implement for small devices as they occupy very small volume. Two novel SCMR topologies were proposed in [17], but their efficiency was only studied for a maximum angular misalignment of 90°. Also, the range and lateral misalignment effects were not examined in [17]. Furthermore, analytical models for SCMR that incorporate misalignment effects were presented in [18]. SCMR's radial and angular misalignment sensitivity were examined in [19] and [20], respectively. Alleviating SCMR's angular misalignment sensitivity is studied in [20] by using tuning circuits, which were not able to maintain high efficiency above 60° of misalignment. Also, it should be pointed out that tuning circuits add the complexity to SCMR RX systems and cannot compensate for large angular and radial misalignments as they cannot recover the lost flux density between TX and RX resonator. However, tuning circuits can be used for compensating the effects of variable axial distance between TX and RX systems [21], [22]. Omnidirectional WPT systems that utilized current phase shifting between power inputs were studied in [23]. These systems utilize two or three separate coils, thereby occupying large volume and also require separate power sources specific phase shift between them. Therefore, these

Manuscript received September 21, 2015; revised February 4, 2016, April 16, 2016, and June 25, 2016; accepted August 17, 2016. Date of publication September 2, 2016; date of current version February 27, 2017. This work was supported by the National Science Foundation under Grant ECCS 1307984, by the Army Research Office under Grant W911NF-13-1-0149, by the Air Force Office of Scientific Research under Grant FA9550-16-1-0145, and by the FIU Graduate School under the Dissertation Year Fellowship. Recommended for publication by Associate Editor M. Duffy.

The authors are with the Department of Electrical and Computer Engineering, Florida International University, Miami, FL 33174 USA (e-mail: ddaer001@fiu.edu; hhu005@fiu.edu; georgako@fiu.edu).

Color versions of one or more of the figures in this paper are available online at http://ieeexplore.ieee.org.

Digital Object Identifier 10.1109/TPEL.2016.2605698

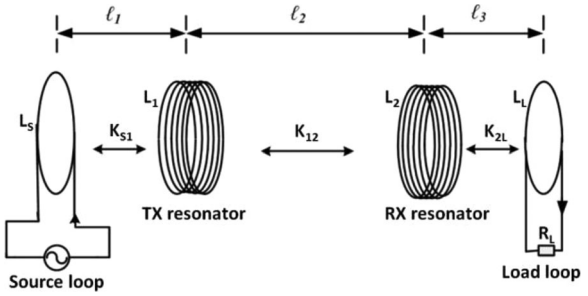

Fig. 1. Schematic of a standard SCMR system.

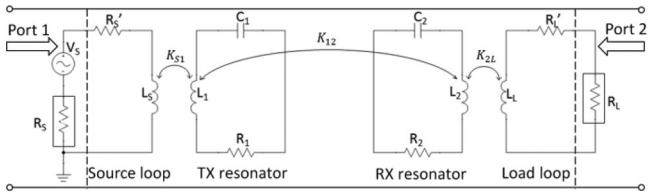

Fig. 2. Equivalent circuit of an SCMR system.

systems are less practical than the WPT systems proposed here, which do not require as large of volume and do not use separate power sources.

It can be seen that previous research efforts have investigated the effects of both angular and lateral misalignment of SCMR systems. However, no solutions, which are based on new geometries of SCMR elements, have been proposed to address the sensitivity of SCMR systems to angular and lateral misalignment. This paper focuses on the design of novel wireless SCMR powering systems that are less sensitive to misalignment compared to traditional SCMR systems. Also, the effects of complete 360° of angular misalignment are studied along with the effects of lateral misalignment. Finally, the range of each system is reported.

II. SCMR WPT and Misalignment Types

The WPT systems proposed in this paper are based on the SCMR method [6]. A typical SCMR system is shown in Fig. 1 and it consists of the following: (a) a transmitter with one source loop where the excitation is connected and a TX resonator coil or loop, and (b) a receiver with one load loop where the load is connected and an RX resonator coil or loop. In order for SCMR to achieve high WPT efficiency the TX and RX resonators must resonate at the same frequency, which also is the frequency where the resonators naturally exhibit the highest *Q*-factor. It is this condition indeed that enables SCMR to achieve WPT efficiencies that are significantly larger than standard two loops or coils inductively coupled or resonant inductively coupled systems. This has been confirmed in [24], in which three types of WPT systems of the same size and operating frequency were compared, namely: 1) a nonresonant inductively coupled system, 2) a resonant inductively coupled system, and 3) an SCMR system. The equivalent circuit of an SCMR system is shown in Fig. 2.

In Fig. 2, R_S and R_L are, respectively, the internal resistances of the input and output ports; R'_S, R_1, R_2, and R'_L are the total resistances of the source loop, TX resonator, RX resonator, and load loop, respectively; L_S, L_1, L_2, and L_L are the corresponding inductances of these loops; C_1 and C_2 are the external capacitors connected to the TX and RX resonator loops; K_{S1}, K_{12}, and K_{2L} are the coupling coefficients between the loops. Also, the input and output ports are shown in Fig. 2. The source loop delivers power to the TX resonator through inductive coupling, and similarly, the RX resonator delivers power to the load loop through inductive coupling. The TX resonator efficiently transfers power to the RX resonator over large distances by satisfying the SCMR condition (i.e., both TX and RX resonators resonate at the same frequency where their *Q*-factor is naturally maximum). The frequency where the *Q*-factor of a loop is maximum can be written as [25]

$$f_{\max} = \frac{c^{8/7}\mu_0^{1/7}\rho^{1/7}}{4\cdot 15^{2/7}\pi^{11/7}r_c^{2/7}r^{6/7}} \tag{1}$$

where μ_0 is the permeability of free space, ρ is the loop's material resistivity, r_c is the cross-sectional radius of the loop, and r is the radius of the loop. In order to design a proper SCMR system that operates at a certain frequency, f_0, with high efficiency, the following equation must be satisfied:

$$f_0 = f_{\max}. \tag{2}$$

Based on (1) and (2), the radii of the TX and RX resonator loops are equal to

$$r = \frac{c^{4/3}\mu_0^{1/6}\rho^{1/6}}{4^{7/6}15^{1/3}\pi^{11/6}r_c^{1/3}f_0^{7/6}}. \tag{3}$$

In order to form resonant TX and RX loops, a lumped capacitor must be connected on each of these loops. This capacitor can be calculated using the following formula:

$$L = \mu_0 r\left[\ln\left(\frac{8r}{r_c}\right) - 2\right] \tag{4}$$

$$C = \frac{1}{(2\pi f_{\max})^2 L} \tag{5}$$

where *L* is the inductance of each TX and RX loop. Therefore, the TX/RX resonators can be designed using (2)–(5). The source and load coils in all of our designs are scaled versions (i.e., have same geometrical shape) of the TX and RX resonator coils. Therefore, the scaling factor that scales the TX (or RX) resonator coil to the source (or load) resonator coil is the only parameter that needs to be determined once the TX and RX resonators are designed. ANSYS HFSS is used to optimize this scaling factor in order to achieve optimal power transfer efficiency. Based on our design experience and simulation results, the size of the source and load coils is typically 3/5 of the resonator size. It has been shown by several papers [7], [20] that the typical distance at which an SCMR system exhibits maximum efficiency is approximately equal to the diameter of the TX and RX resonators.

Coil orientation and alignment are critical in the design of efficient SCMR systems. In fact, conventional SCMR systems exhibit high sensitivity to angular misalignment. In Fig. 3, a typical standard SCMR system is shown along with the definition of azimuth and elevation misalignment angles. In Fig. 3, ℓ_1 is the distance between the source element and the TX resonator,

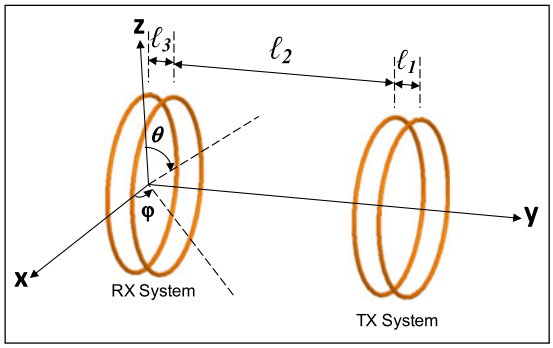

Fig. 3. SCMR system illustrating azimuth and elevation misalignment angles, φ and θ, respectively.

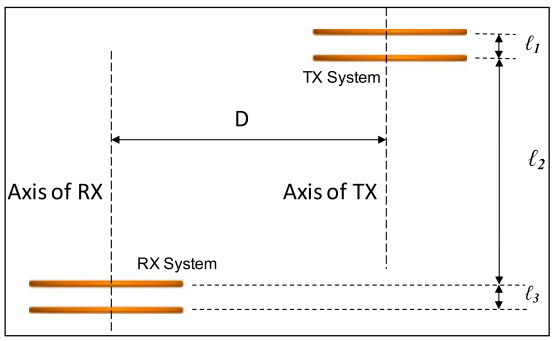

Fig. 4. SCMR system with lateral misalignment.

ℓ_2 is the distance between the TX and RX resonators, and ℓ_3 is the distance between the RX resonator and the load element. In what follows, we explain the different types of misalignment cases that are critical for the performance of SCMR-based WPT systems.

For the angular azimuth and elevation misalignment studies presented here, the source loop and transmitter resonator stay still, while the load loop and RX resonator are simultaneously rotated together around the transmitter.

A. Angular Azimuth Misalignment

In this case, the RX system (RX resonator and load element) rotates in the *xy* plane around the *z*-axis from $\phi = 0°$ to 360, while the TX system (TX resonator and source element) is fixed.

B. Angular Elevation Misalignment

In this case, the RX system is rotated in the *yz* plane (i.e., elevation plane) from $\theta = 0°$ to 360 around the *x*-axis, while the TX system is fixed.

C. Lateral Misalignment

In this case, the RX system is misaligned by moving it parallel to the TX system, while the distance between the planes of the RX and TX systems, ℓ_2, is kept constant. The lateral misalignment offset distance, *D*, is shown in Fig. 4.

III. Misalignment Analysis

In this section, the performance of standard SCMR systems will be compared to the performance of novel SCMR systems

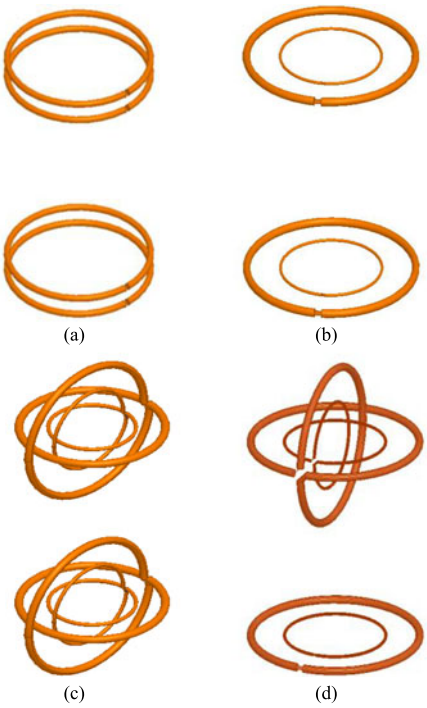

Fig. 5. Different SCMR systems. (a) Standard SCMR with parallel loops elements. (b) CSCMR. (c) 3-D SCMR. (d) HSCMR.

(which will be introduced in this paper) for various misalignment conditions. Standard SCMR systems consist of four elements and require that TX and RX systems are aligned in order to achieve high efficiency. In fact, such standard SCMR systems suffer a significant decrease of their wireless powering efficiency when they are misaligned. The high sensitivity of standard SCMR to misalignment is a major disadvantage for many applications, such as implantable or wearable devices, biosensors, and other mobile devices, where alignment between TX and RX systems not only cannot be guaranteed but also constantly changes due to movement or mobility. Hence, there is a need for new misalignment insensitive and highly efficient SCMR design that can solve this practical problem.

Fig. 5(a) shows a standard SCMR system whereas our proposed novel SCMR systems, which are less sensitive to misalignment, are shown in Fig. 5(b)–(d). The performance of these SCMR systems is examined in this section for the different misalignment conditions described in Section II. All the simulations in this paper were performed using version 16.0.0 of ANSYS HFSS [26] and Designer [27]. All SCMR resonators examined below were designed to resonate at the frequency where their *Q*-factor is maximum, which was accomplished by using analytical equations for the standard loops and simulations for the proposed 3-D loops.

The entire WPT system is considered as a two-port network. It is assumed in all our designs that the source and load impedances are 50 Ω. Therefore, in this paper, the following quantity is defined as

$$G_T = \text{Matched Transducer Power Gain} = |S_{21}|^2 \qquad (6)$$

in order to compare the performance of different SCMR systems. Also, the quantity of angle range is defined, as the total

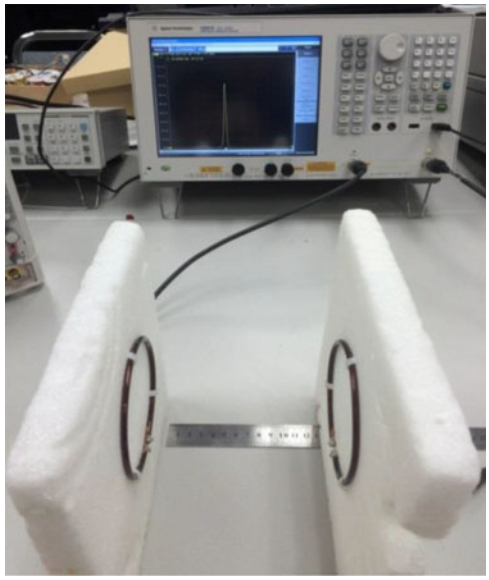

Fig. 6. Prototype of a standard SCMR system.

range of angles for which the G_T is above a specified level. In addition, the new quantity of lateral range is defined, as the maximum lateral misalignment distance for which the G_T is above a specified level.

The gain G_T of our prototypes is measured using network analyzer based on the *S*-parameters. Ports 1 and 2 of the network analyzer are connected to the transmitter and the receiver, respectively, and the *S*-parameters are measured. Then, the data of the measured G_T are obtained by programming directly the equation $|\mathrm{S}_{21}|^2$ on the network analyzer.

A. Standard SCMR

First, the performance of the conventional SCMR topology, which is shown in Fig. 5(a), is examined under different misalignment conditions. For angular azimuth rotation, the RX system rotates in the *xy* plane around the *z*-axis, while the TX system is fixed. For angular elevation rotation, the RX system is rotated in the *yz* plane around *x*-axis, while the TX system is fixed.

A standard SCMR system was designed for optimal performance following the equations presented in [25], and its prototype is shown in Fig. 6. The specifications of this SCMR system are as follows: the radius of the four loops is $r_1 = 50\,\mathrm{mm}$ and their cross-sectional radius is $r_c = 2.2\,\mathrm{mm}$; $\ell_1 = \ell_3 = 23\,\mathrm{mm}$, and $\ell_2 = 120\,\mathrm{mm}$. An 18-pF capacitor is needed to achieve maximum G_T, and the operating frequency is 85.7 MHz.

Fig. 7 shows the simulated and measured G_T of this standard SCMR system under the different misalignment conditions described in Section II. Fig. 7 clearly demonstrates the high sensitivity of conventional SCMR systems on the angular misalignment between TX and RX systems. Also, it can be seen that $|S_{21}|^2$ drops rapidly for lateral misalignment distances that are greater than 40 mm. In what follows, the angle range and lateral range are reported based on the measured data. The results of Fig. 7 illustrate that SCMR's angle range for a $|S_{21}|^2$ level, which is set at 60% of its maximum, is 102° for both azimuth and elevation misalignment. The angle range for a $|S_{21}|^2$ level, which is set at 30% of its maximum, is 278° for both azimuth and elevation misalignment. The lateral range for a $|S_{21}|^2$ level, which is set at 30% of its maximum, is 78 mm. Also the G_T of this standard SCMR system exhibits two nulls at misalignment angles (azimuth or elevation) of 75° and 285°. Fig. 8 illustrates the range of this system.

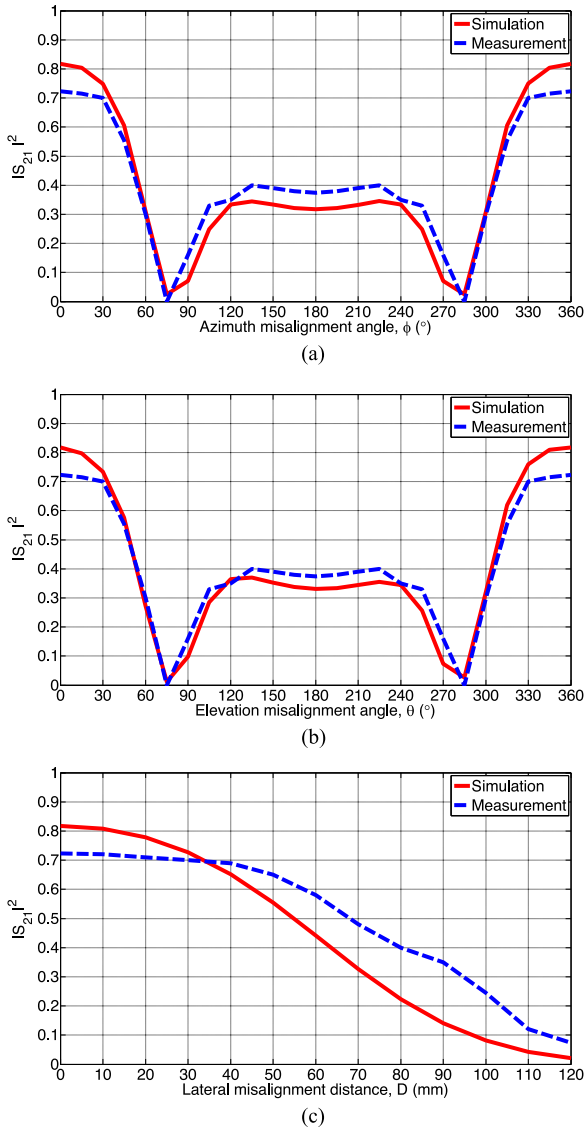

Fig. 7. G_T of the standard SCMR system of Fig. 5(a) under different misalignment conditions. (a) Angular azimuth misalignment. (b) Angular elevation misalignment. (c) Lateral misalignment.

B. CSCMR

The misalignment sensitivity of CSCMR system is studied here. For angular azimuth rotation, the RX system rotates in the *xy* plane around the *z*-axis, while the TX system is fixed. For angular elevation rotation, the RX system is rotated in the *yz* plane around the *x*-axis, while the TX system is fixed. In a

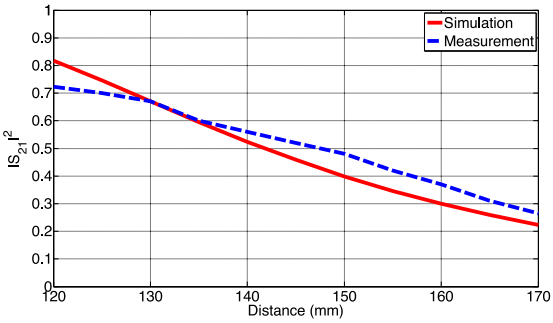

Fig. 8. G_{T} of standard SCMR versus distance.

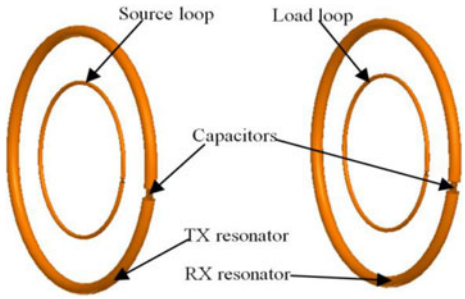

Fig. 9. Schematic of CSCMR system.

CSCMR system, the source loop and load loop are embedded into the TX and RX resonators, respectively. Therefore, the source loop is coplanar with the TX resonator and the load loop is coplanar with the RX resonator (see Fig. 9). A standard SCMR system requires a separation between the source and the TX resonator as well as between the load and the RX resonator. Therefore, standard SCMR systems occupy significant volume and cannot be easily implemented in various applications. On the other hand, a CSCMR system has a source loop that is concentric and coplanar with the TX resonator (as well as a load loop that is concentric and coplanar with the RX resonator). Therefore, CSCMR systems are easier to implement for small devices. Furthermore, CSCMR is less sensitive to misalignment as our results will show in this section.

A CSCMR system is designed (see Fig. 10) with the following specifications: TX and RX resonators have a radius of 50 mm and a cross-sectional radius of 2.2 mm; the source and load loops have a radius of 30 mm and a cross-sectional radius of 0.8 mm; the distance between the TX and RX resonators is 120 mm. A 22-pF capacitor is connected to both TX and RX resonators in order for this system to operate at 76.2 MHz.

Fig. 11 illustrates the G_T of this CSCMR system for different misalignment conditions. Fig. 11 shows that the G_T exhibits two nulls at 90° and 270° of azimuth or elevation misalignment. Furthermore, as the misalignment angle (azimuth or elevation) increases from 90° and 270° (null-to-null), CSCMR's G_T increases from zero to its maximum and then reduces back to zero; this is an improvement compared to the performance of standard SCMR. Specifically, as shown in Fig. 7, as the misalignment angle (azimuth or elevation) increases from 75° to 285° (null-to-null), standard SCMR's G_{T} increases from zero to only half

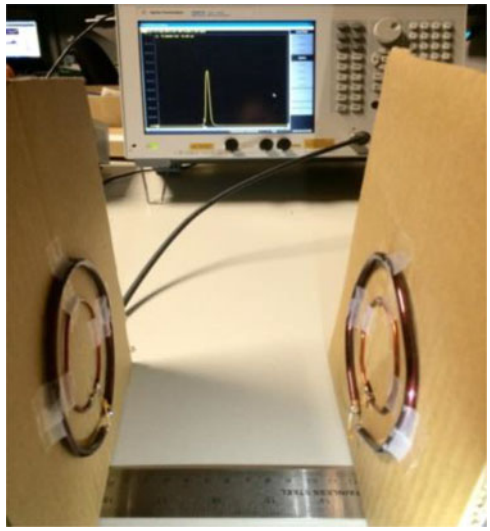

Fig. 10. Prototype of CSCMR system.

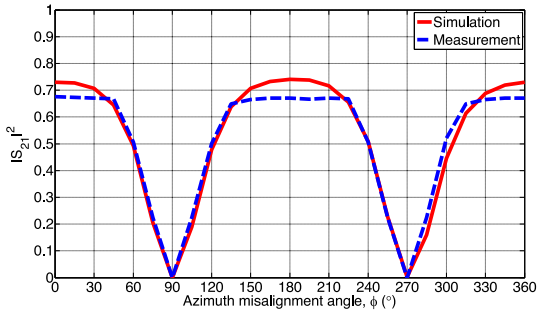

(a)

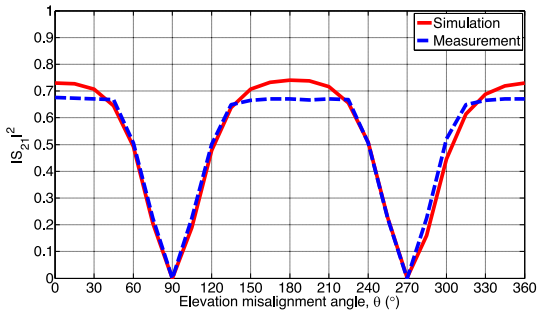

(b)

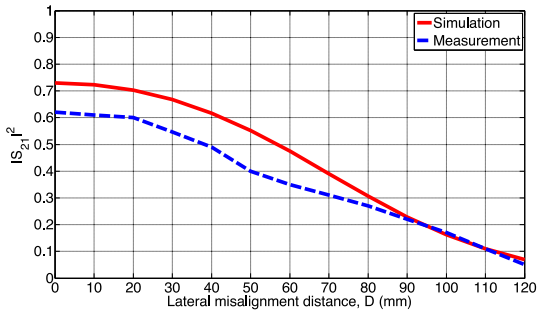

(c)

Fig. 11. G_{T} of CSCMR system of Fig. 5(b) under different misalignment conditions. (a) Angular azimuth misalignment. (b) Angular elevation misalignment. (c) Lateral misalignment.

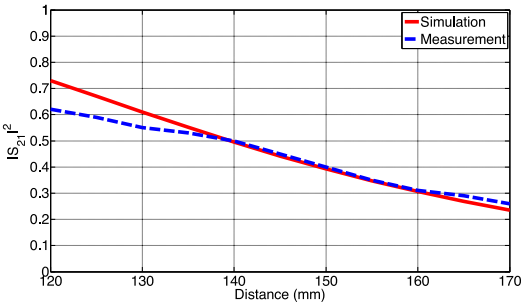

Fig. 12. G_T of CSCMR versus distance.

of its maximum and then reduces back to zero. Therefore, by comparing Figs. 7 and 11, it can be concluded that CSCMR is less sensitive to azimuth and elevation misalignment than standard SCMR. Also, the results in Fig. 11 illustrate that CSCMR is reversible (i.e., operates with the same G_T when it is rotated in the azimuth or elevation plane by 180°), whereas standard SCMR is not. This occurs due to the geometrical symmetry of CSCMR systems.

In what follows, the angle range and lateral range are reported based on the measured data. The angle range of this CSCMR system for a $|S_{21}|^2$ level, which is set at 60% of its maximum, is 248° for both azimuth and elevation misalignment and is significantly larger than the one (i.e., 102°) of standard SCMR. Also, the angle range of this CSCMR system for an $|S_{21}|^2$ level, which is set at 30% of its maximum, is 294° for both azimuth and elevation misalignment and is larger than the one (i.e., 278°) of standard SCMR. Furthermore, the lateral range for a $|S_{21}|^2$ level, which is set at 30% of its maximum, is 92 mm, and it is larger than the one (i.e., 78 mm) of standard SCMR. Therefore, it can be concluded that CSCMR is also less sensitive to lateral misalignment than standard SCMR. The G_T of this CSCMR system exhibits two nulls at misalignment angles of 90° and 270°. Finally, the range of this CSCMR design is shown in Fig. 12, and it is similar to the one of standard SCMR.

Based on the results of Fig. 11(a) and (b), CSCMR systems exhibit the same variation of $|S_{21}|^2$ for angular azimuth and elevation misalignment. This was also the case for SCMR systems, as shown in Fig. 7(a) and (b). Comparing the results for the CSCMR and SCMR systems, it can be concluded that they both have similar variations except for the G_T from 120° to 240° of misalignment. Specifically, the standard SCMR system exhibits a G_T of only 30–40% for 120° to 240° of misalignment, whereas the CSCMR system exhibits a G_T above 50% in the same range of misalignment angles. Also, it is observed by comparing Fig. 11(a) and (b) with Fig. 7(a) and (b) that the G_T of the CSCMR system raises back to its maximum value between its nulls, whereas the G_T of the standard SCMR drops to a significantly lower value between its nulls. Therefore, the CSCMR system exhibits significantly less misalignment sensitivity and better performance compared to standard SCMR.

C. Three-Dimensional SCMR

A novel SCMR system is proposed here, and it is shown in Fig. 13. In this SCMR system, the TX and RX resonator elements as well as the source and load elements are 3-D loops consisting of two continuous connected orthogonal loops. The TX and RX systems in 3-D SCMR systems are identical. Therefore, one of them is shown in Fig. 13. The source (or load) loop, the TX (or RX) resonator, and the capacitor connected at the port of the TX (or RX) resonator are shown in Fig. 13. The input power (or load) is connected to the source (or load) loop, as shown in Fig. 13. The source (or load) loop has the same geometry as the TX (or RX) resonator. In fact, the source (or load) loop is a scaled version of the TX (or RX) resonator. The source (or load) loop and the TX (or RX) resonator loop are isolated from each other (i.e., they are not directly connected), and each of them is constructed by a single continuous copper wire that is bend accordingly to provide the 3-D geometry shown in Fig. 13. Also, each of these 3-D loops consists of two orthogonal loops connected in series. The 3-D TX and RX resonator loops are designed so that they exhibit their highest *Q*-factor at the frequency of operation. Capacitors are connected at their feed point to resonate them at the operating frequency. In addition, the source and load loops are concentrically embedded into the TX and RX resonators, respectively. This type of system has a spherical symmetry, and therefore, it is expected to be less sensitive to misalignment. The angular misalignment rotations are performed as follows: for angular azimuth rotation, the RX system rotates in the *xy* plane around the *z*-axis, while the TX system is fixed; for angular elevation rotation, the RX system is rotated in the *yz* plane around the *x*-axis, while the TX system is fixed.

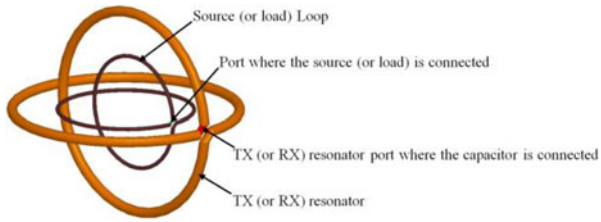

Fig. 13. Three-dimensional SCMR TX or RX system.

Fig. 14. Prototype of the 3-D SCMR system.

A 3-D SCMR system is designed (see Fig. 14) and its geometric specifications are described in what follows. The TX and RX resonators are comprised of two connected orthogonal loops with the following radii: the radius of the outer loop is $r_1 = 50$ mm, the radius of the inner loop is $r_2 = 45$ mm, and the cross-sectional radius of both loops is

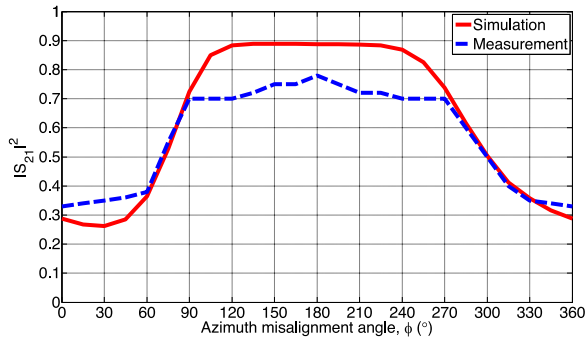

(a)

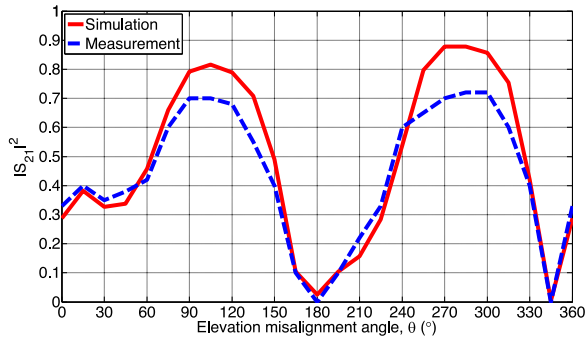

(b)

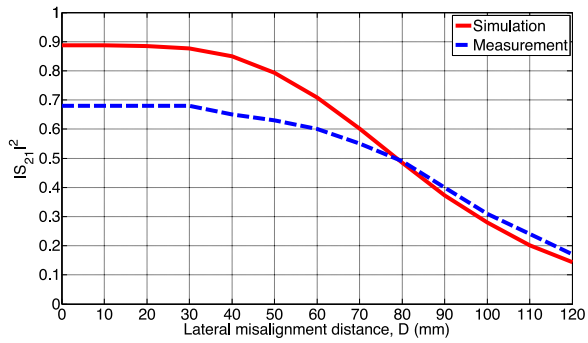

(c)

Fig. 15. G_T of 3-D SCMR system of Fig. 5(c) under different misalignment conditions. (a) Angular azimuth misalignment. (b) Angular elevation misalignment. (c) Lateral misalignment.

$r_c = 2.2$ mm. The source and load elements are comprised of two connected orthogonal loops with the following radii: the radius of the outer loop is $r_3 = 30$ mm, the radius of the inner loop is $r_4 = 25$ mm, and the cross-sectional radius of both loops is $r_c' = 0.8$ mm. The distance between the TX and RX systems is $\ell_2 = 120$ mm and it is defined as the distance from the center of the TX resonator to the center of the RX resonator. The frequency of operation is 80.2 MHz. Each of the TX and RX resonators are connected to a 10-pF capacitor. This capacitance value was found by simulation analysis so that maximum G_T is achieved by this system.

Fig. 15 illustrates the G_T of this 3-D SCMR system under different misalignment conditions. Specifically, Fig. 15(a) shows that for azimuth misalignment, the G_T of this 3-D SCMR system does not exhibit any nulls and it remains above 30% for the full range of 360° of azimuth misalignment. This is a clear advantage of this system over standard SCMR and CSCMR systems. However, Fig. 15(b) shows that for elevation misalignment, the G_T of this 3–D SCMR system exhibits two nulls at 180° and 345° and similar variation with the G_T of CSCMR system shown in Fig. 11(b). Some of the difference between measurements and simulations can be attributed to the fact that prototypes were manually constructed and therefore, they are not exactly the same with simulation models. Especially, these 3-D loops are difficult to construct by hand and generate perfectly circular geometries. Also, the capacitors used in our prototypes have some losses and are not perfect as the capacitors used in the simulation, which contributes a slight drop in the measured G_{T} compared to the simulated one.

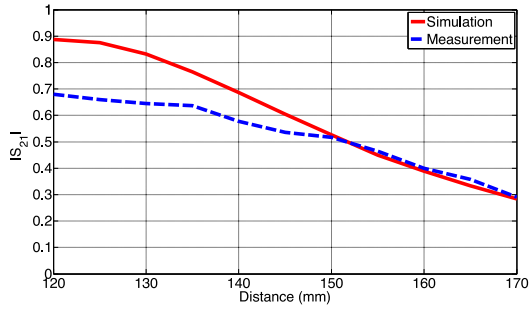

Fig. 16. G_T of 3-D SCMR versus distance.

Even though in this case the transmitter and receiver are identical, Fig. 15(a) is different from Fig. 15(b) because the portions of the 3-D loops that are aligned during rotation in the azimuth misalignment are different from the ones in the elevation misalignment. Also, Fig. 15(b) is not perfectly symmetric because each 3-D loop is not perfectly symmetric. In fact, each 3-D loop is composed by two 2-D loops that are connected in series and certain geometric modifications have to be done to avoid shorting of the 2-D loops at the port, which in turn result in nonperfectly symmetric 3-D loops.

Based on the measured data, the angle ranges of this 3-D SCMR system for an $|S_{21}|^2$ level, which is set at 60% of its maximum, are 221° and 168° for azimuth and elevation misalignment, respectively. These angle ranges are less than the corresponding ones of CSCMR (i.e., 248°). However, the angle ranges of this 3-D SCMR system for an $|S_{21}|^2$ level, which is set at 30% of its maximum, are 360° and 272° for azimuth and elevation misalignment, respectively; therefore, they are larger than the corresponding ones of CSCMR (i.e., 294°) and standard SCMR (i.e., 278°). From Fig. 15(c), it can be seen that the lateral range for an $|S_{21}|^2$ level, which is set at 30% of its maximum, is 102 mm, and it is larger than the one (i.e., 92 mm) of CSCMR. This shows that 3-D SCMR is less sensitive to lateral misalignment performance than both standard SCMR and CSCMR.

The range of this 3-D SCMR system is shown in Fig. 16. By comparing Fig. 16 with Figs. 8 and 12, it can be seen that 3-D SCMR exhibit longer range than SCMR and CSCMR. Specifically, at a distance of 170 mm, the G_{T} of 3-D SCMR is 30% versus the 20% G_{T} of both standard SCMR and CSCMR.

The 3-D SCMR system is less sensitive to misalignment comparing to standard SCMR and CSCMR systems. Specifically,

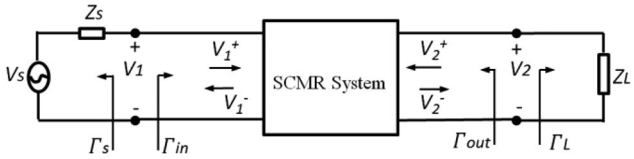

Fig. 17. Two-port network for SCMR system with source and load impedances.

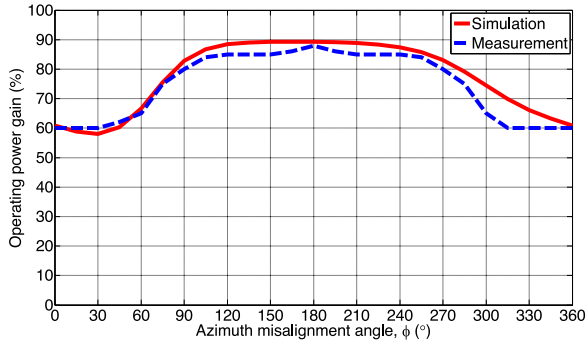

Fig. 18. Operating power gain of 3-D SCMR.

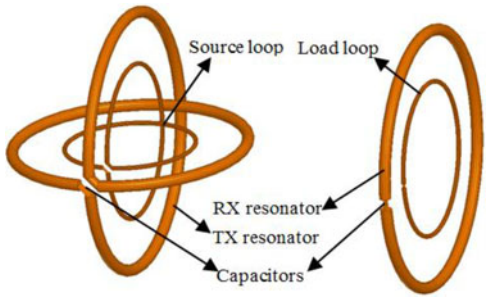

Fig. 19. Schematic of the HSCMR system.

3-D SCMR achieves misalignment insensitivity for azimuth angular rotation for the entire 360° of rotation as shown in Fig. 15(a). Also, the G_T of the 3-D SCMR system is above 70% for 90° to 270° of azimuth misalignment, whereas the G_{T} of the standard SCMR is less than 40% for the same range of misalignment. The maximum G_T of standard SCMR, CSCMR and 3-D SCMR are 80%, 75%, and 88% for the angular azimuth misalignment respectively. For angular elevation rotation, standard SCMR, CSCMR, and 3-D SCMR systems all exhibit two nulls in the G_T. These nulls are near 90° and 270° for standard SCMR and CSCMR systems, and 180° and 345° for the 3-D SCMR system. The maximum G_{T} for standard SCMR, CSCMR, and 3-D SCMR for the angular elevation misalignment are 80%, 75%, and 86%, respectively.

In order to quantify the SCMR's system efficiency, the operating power gain is used since it includes the effects of the reflection coefficient. The operating power gain is defined as the ratio of power dissipated at the load to the power delivered at the input of the two-port network, which is also the power input at the transmitter coil. The entire SCMR WPT system is considered as a two-port network. In order to better understand the power gain definition, this two-port network with source and load impedance is shown in Fig. 17.

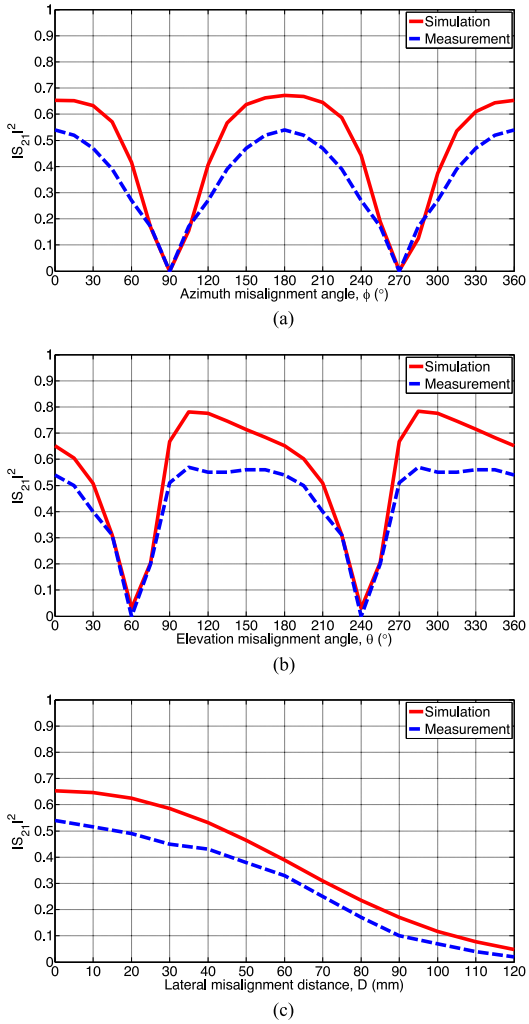

Fig. 20. G_T of the HSCMR system of Fig. 5(d) under different misalignment conditions. (a) Angular azimuth misalignment. (b) Angular elevation misalignment. (c) Lateral misalignment.

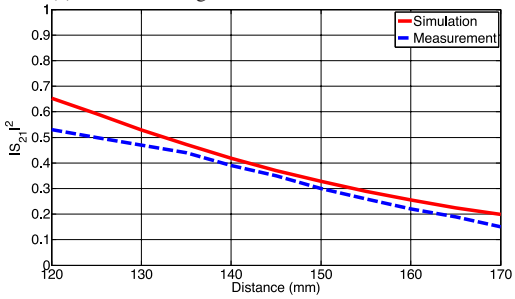

Fig. 21. G_T of HSCMR versus distance.

The operating power gain can be defined in terms of S-parameters per [28] as follows:

$$\mathrm{Gain}_O = \frac{P_L}{P_{\mathrm{in}}} = \frac{|S_{21}|^2\left(1-|\Gamma_L|^2\right)}{\left(1-|\Gamma_{\mathrm{in}}|^2\right)|1-S_{22}\Gamma_L|^2} \tag{7}$$

where Γ_L is the reflection coefficient at the load

$$\Gamma_L = \frac{Z_L - Z_0}{Z_L + Z_0} \tag{8}$$

TABLE I
COMPARISON OF DIFFERENT SCMR SYSTEMS

		Angle Misalignment Range (°) 60%	Angle Misalignment Range (°) 30%	Lateral range (mm) 30%
Standard SCMR	Azimuth	102	278	78
	Elevation	102	278	
Conformal SCMR	Azimuth	248	294	92
	Elevation	248	294	
3-D SCMR	Azimuth	221	360	102
	Elevation	168	272	
Hybrid SCMR	Azimuth	241	290	86
	Elevation	259	306	

and

$$\Gamma_{\text{in}} = S_{11} + \frac{S_{12}S_{21}\Gamma_L}{1 - S_{22}\Gamma_L}. \tag{9}$$

Assuming the SCMR system is terminated to a 50-Ω load and according to (8), $\Gamma_L = 0$, which in turn according to (9) makes $\Gamma_{in} = S_{11}$. In this case, the operating power gain is written as

$$\text{Gain}_O = \frac{|S_{21}|^2}{1 - |S_{11}|^2}. \tag{10}$$

Fig. 18 illustrates the simulated and measured operating power gain based on (10) for the 3-D SCMR for the azimuth misalignment case. By comparing Figs. 15(a) and 18, it can be observed that the operating power gain and the G_T exhibit similar variation versus the azimuth misalignment angle, but the amplitude of the operating gain is larger since it takes into account the reflection coefficient, S_{11}, at the input of the SCMR system. It should be noted that since this efficiency formula is based on a 50-Ω load impedance, additional circuit blocks are needed if other load impedances are used.

D. Hybrid SCMR (HSCMR)

In this section, the previous two models of CSCMR and 3-D SCMR are combined into one system called HSCMR as shown in Fig. 5(d). Specifically, the receiver is a CSCMR element, whereas the transmitter is a 3-D SCMR element. Therefore, since this HSCMR system has a receiver that is conformal, it is easier to implement it in practice than the 3-D SCMR system. Also, this HSCMR system has a transmitter that exhibits spherical symmetry. The angular misalignment rotations are performed as follows: for angular azimuth rotation, the RX system rotates in the *xy* plane around the *z*-axis, while the TX system is fixed; for angular elevation rotation, the RX system is rotated in the *yz* plane around the *x*-axis, while the TX system is fixed.

An HSCMR system is designed (see Fig. 19) and its geometric specifications are described in what follows. For the TX system's 3-D resonator, the radius of the outer loop is $r_1 = 50\,\text{mm}$, the radius of the inner loop is $r_2 = 45\,\text{mm}$, and the cross-sectional radius of both loops is $r_c = 2.2\,\text{mm}$. The 3-D source element is comprised of two connected orthogonal loops with the following specifications: the radius of its outer loop is $r_3 = 30\,\text{mm}$, the radius of its inner loop is $r_4 = 25\,\text{mm}$, and the cross-sectional radius of both loops is $r_c' = 0.8\,\text{mm}$. A 10-pF capacitor is needed for the transmitter. The conformal RX system has the following geometric specifications: the radius of the outside loop is 50 mm with cross-sectional radius of 2.2 mm; the radius of the inside loop is 30 mm with cross-sectional radius of 0.8 mm. A 19.9-pF capacitor is connected on the RX resonator provide the best G_T. The operating frequency of this HSCMR system is 80.2 MHz. The distance between the center of TX and RX systems is 120 mm.

Fig. 20 illustrates the G_T of this HSCMR system for different misalignment conditions. Fig. 20(a) illustrates that the variation of HSCMR's G_T for azimuth misalignment is similar to the variation of CSCMR shown in Fig. 11(a), i.e., the G_{T} has two nulls at 90° and 270°, and it raises to its maximum between the nulls. Fig. 20(b) shows that HSCMR's G_T for elevation misalignment has two nulls that are shifted by 30° lower compared to its nulls for azimuth misalignment. This can be useful in case WPT needs to be achieved at a 90° elevation angular misalignment. The misalignment results of HSCMR illustrate that it performs similarly to the CSCMR, since they both use the same type of receiver. The only difference is that the nulls of the G_T shift from 90° and 270° for the CSCMR to 60° and 240° for the HSCMR due to the fact that the HSCMR transmitter has two orthogonal loops that can couple with the receiver.

The angle ranges of this HSCMR system for an $|S_{21}|^2$ level, which is set at 60% of its maximum, are 241° and 259° for azimuth and elevation misalignment, respectively. HSCMR angle ranges are similar to the ones of CSCMR (i.e., 248°) but larger than the ones of 3-D SCMR (i.e., 221° and 168°). The angle ranges for an $|S_{21}|^2$ level, which is set at 30% of its maximum, are 290° and 306° for azimuth and elevation misalignment, respectively, which are again similar to the ones of CSCMR (i.e., 294°). Fig. 20(c) illustrates that the lateral range for an $|S_{21}|^2$ level, which is set at 30% of its maximum, is 86 mm, which is smaller than the ones of CSCMR (i.e., 92 mm) and 3-D SCMR (i.e., 102 mm) but larger than the one of standard SCMR (i.e., 78 mm). Fig. 21 depicts the G_{T} of HSCMR versus distance. By comparing Fig. 21 with the corresponding figures for the other WPT systems presented above, it can be concluded that HSCMR's range is less than the one of 3-D SCMR but similar to the one of CSCMR.

IV. CONCLUSION

This paper proposed various novel topologies of SCMR systems that are less sensitive to misalignment between TX and RX systems than standard SCMR system. From the results shown above, it can be concluded that CSCMR exhibits less sensitivity to misalignment since its G_T between the angles where the nulls occur increases back to its maximum, whereas for standard SCMR, its G_T drops to a significantly lower value between its nulls. This is due to the fact that the source and load loops are embedded concentrically in the TX and RX resonators, respectively. Therefore, when the CSCMR RX system is rotated to 180° of misalignment, its position compared to the TX system is exactly the same as its position for 0° misalignment. On the other hand, standard SCMR uses a pair of parallel loops at each of the TX and RX systems, which results reduced G_{T} when the

RX is rotated to 180° of misalignment. In addition, 3-D SCMR exhibits no nulls for azimuth misalignment, which is a significant improvement over the standard SCMR and CSCMR. This happens because each of the loops of 3-D SCMR is constructed using two orthogonal loops connected in series; therefore, for any angle of rotation, two pairs of loops (one at the TX and one at the RX system) are always coupled. For the elevation rotation, 3-D SCMR exhibits two nulls at 180° and 345°, which can be attributed to the cancelation of the magnetic fluxes received by the two orthogonal loops at these two angles. HSCMR performs similarly to CSCMR since they both use the same receiver. The only difference is that the nulls of the G_T shift from 90° and 270° for the CSCMR to 60° and 240° for the HSCMR due to the fact that the HSCMR transmitter has two orthogonal loops that can couple with the receiver.

Table I summarizes the measured results presented above and compares the performance of the different SCMR systems. The angle misalignment ranges for azimuth and elevation misalignment are calculated based on the angles, for which the G_T maintains a value above 60% or 30% of the maximum G_{T} of each system. It can be seen that all three proposed SCMR systems (i.e., CSCMR, 3-D SCMR, and HSCMR) exhibit larger angle misalignment range compared to standard SCMR. In fact, 3-D SCMR exhibits the best performance regarding misalignment since it has no G_T nulls over the entire 360° azimuth rotation. Furthermore, an HSCMR system was proposed in an effort to provide a WPT system that has a conformal receiver, which maybe more suitable for certain applications. This HSCMR system is also less sensitive to misalignment compared to standard SCMR.

REFERENCES

[1] J. Lee and B. Han, "A bidirectional wireless power transfer EV charger using self-resonant PWM," *IEEE Trans. Power Electron.*, vol. 30, no. 4, pp. 1784–1787, Apr. 2015.

[2] K. Finkenzeller, *RFID Handbook: Fundamentals and Applications in Contactless Smart Cards and Identification*, 2nd ed. New York, NY, USA: Wiley, 2003, pp. 65–112.

[3] P. V. Nikitin, K. V. S. Rao, and S. Lazar, "An overview of near field UHF RFID," in *Proc. RFID IEEE Int. Conf.*, Mar. 2007, pp. 167–174.

[4] D. Ahn and S. Hong, "Wireless power transmission with self-regulated output voltage for biomedical implant," *IEEE Trans. Ind. Electron.*, vol. 61, no. 5, pp. 2225–2235, May 2014.

[5] K. Chang-Gyun, S. Dong-Hyun, Y. Jung-Sik, P. Jong-Hu, and B. H. Cho, "Design of a contactless battery charger for cellular phone," *IEEE Trans. Ind. Electron.*, vol. 48, no. 6, pp. 1238–1247, Dec. 2001.

[6] A. Kurs, A. Karalis, R. Moffatt, J. D. Joannopoulos, P. Fisher, and M. Soljacic, "Wireless energy transfer via strongly coupled magnetic resonances," *Science*, vol. 317, pp. 83–85, 2007.

[7] A. Karalis, J. D. Joannopoulos, and M. Soljacic, "Efficient wireless non-radiative mid-range energy transfer," *Ann. Phys.*, vol. 323, pp. 34–48, Jan. 2008.

[8] B. L. Cannon, J. F. Hoburg, D. D. Stancil, and S. C. Goldstein, "Magnetic resonant coupling as a potential means for wireless power transfer to multiple small receivers," *IEEE Trans. Power Electron.*, vol. 24, no. 7, pp. 1819–1825, Jul. 2009.

[9] O. Jonah and S. V. Georgakopoulos, "Wireless power transmission to sensors embedded in concrete via magnetic resonance," in *Proc. IEEE 12th Annu. Wireless Microw. Tech. Conf.*, Apr. 2011, pp. 1–6.

[10] T. C. Beh, M. Kato, T. Imura, S. Oh, and Y. Hori, "Automated impedance matching system for robust wireless power transfer via magnetic resonance coupling," *IEEE Trans. Ind. Electron.*, vol. 60, no. 9, pp. 3689–3698, Sep. 2013.

[11] D. Ahn and S. Hong, "A transmitter or a receiver consisting of two strongly coupled resonators for enhanced resonant coupling in wireless power transfer," *IEEE Trans. Ind. Electron.*, vol. 61, no. 3, pp. 1193–1203, Mar. 2014.

[12] S. G. Lee, H. Hoang, Y. H. Choi, and F. Bien, "Efficiency improvement for magnetic resonance based wireless power transfer with axial-misalignment," *Electron. Lett.*, vol. 48, no. 6, pp. 339–340, Mar. 15, 2012.

[13] W. Zhong and S. Y. R. Hui, "Auxiliary circuits for power flow control in multifrequency wireless power transfer systems with multiple receivers," *IEEE Trans. Power Electron.*, vol. 30, no. 10, pp. 5902–5910, Oct. 2015.

[14] D. Ahn and S. Hong, "Effect of coupling between multiple transmitters or multiple receivers on wireless power transfer," *IEEE Trans. Ind. Electron.*, vol. 60, no. 7, pp. 2602–2613, Jul. 2013.

[15] K. Fotopoulou and B. W. Flynn, "Wireless power transfer in loosely coupled links: Coil misalignment model," *IEEE Trans. Magn.*, vol. 47, no. 2, pp. 416–430, Feb. 2011.

[16] O. Jonah, S. V. Geogakopoulos, and M. M. Tentzeris, "Strongly coupled wireless power transfer with conformal structures," in *Proc. 29th Annu. Rev. Progress Appli. Comput. Electromagn.*, Monterey, CA, Mar. 24–28, 2013, pp. 945–950.

[17] O. Jonah, S. V. Georgakopoulos, and M. M. Tentzeris, "Orientation insensitive power transfer by magnetic resonance for mobile devices," in *Proc. IEEE Wireless Power Transfer*, May 15–16, 2013, pp. 5–8.

[18] W. Junhua, S. L Ho, W. N. Fu, and S. Mingui, "Analytical design study of a novel witricity charger with lateral and angular misalignments for efficient wireless energy transmission," *IEEE Trans. Magn.*, vol. 47, no. 10, pp. 2616–2619, Oct. 2011.

[19] F. Zhang, S. A. Hackwoth, X. Liu, L. Chengliu, and S. Mingui, "Wireless power delivery for wearable sensors and implants in body sensor networks," in *Proc. 2010 Annu. Int. Conf. IEEE Eng. Med. Biol. Soc.*, Aug. 31–Sep. 4, 2010, pp. 692–695.

[20] A. Sample, D. Meyer, and J. Smith, "Analysis, experimental results and range adaptation of magnetically coupled resonators for wireless power transfer," *IEEE Trans. Ind. Electron.*, vol. 58, no. 2, pp. 544–554, Feb. 2011.

[21] H. Qiang, X. Huang, L. Tan, Q. Ji, and J. Zhao, "Achieving maximum power transfer of inductively coupled wireless power transfer system based on dynamic tuning control," *Sci. China Technol. Sci.*, vol. 55, no. 7, pp. 1886–1893, Jul. 2012.

[22] Y. Endo and Y. Furukawa, "Proposal for a new resonance adjustment method in magnetically coupled resonance type wireless power transmission," in *Proc. IEEE MTT-S Int. Microw. Workshop Ser. Innovative Wireless Power Transmiss.: Technol., Syst., Appl.*, May 10–11, 2012, pp. 263–266.

[23] W. Ng, C. Zhang, D. Lin, and S. Y. R. Hui, "Two- and three-dimensional omnidirectional wireless power transfer," *IEEE Trans. Power Electron.*, vol. 29, no. 9, pp. 4470–4474, Sep. 2014.

[24] O. Jonah and S. V. Georgakopoulos, "Wireless power transmission to sensors embedded in concrete via magnetic resonance," in *Proc. Wireless Microw. Tech. Conf.*, Apr. 18–19, 2011, pp. 1–6.

[25] O. Jonah, S. V. Georgakopoulos, and M. M. Tentzeris, "Optimal design parameters for wireless power transfer by resonance magnetic," *IEEE Antennas Wireless Propag. Lett.*, vol. 11, pp. 1390–1393, 2012.

[26] (2016). [Online]. Available: http://www.ansys.com/Products/Electronics/ANSYS-HFSS

[27] (2016). [Online]. Available: http://resource.ansys.com/Products/Simulation+Technology/Electronics/RF+&+Microwave/ANSYS+DesignerRF/Features/ANSYS+Nexxim+Circuit+Solver+Technology+ANSYS+DesignerRF

[28] D. M. Pozar, "Microwave engineering," in *Microwave Amplifier Design*, 4th ed. Hoboken, NJ, USA: Wiley, 2011, pp. 558–563.

Daerhan Liu (S'13) received the B.S. degrees in electrical engineering from the University of Science and Technology Beijing, Beijing, China, in 2011, and the M.S. degree in electrical engineering from Florida International University, Miami, FL, USA, in 2013, where he is currently working toward the Ph.D. degree in the Department of Electrical and Computer Engineering.

He is a Research Assistant in the ElectroMagnetic Laboratory, Florida International University. His research interests include misalignment insensitive wireless power transfer systems using strongly coupled magnetic resonance (SCMR) method, combining wireless power and data transfer via SCMR, and the effect of metal surface on conformal SCMR performance.

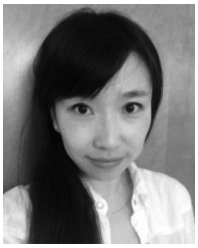

Hao Hu (S'12) received the B.S. and M.S. degrees in electrical engineering from Xi'an Jiaotong University, Xi'an, China, in 2006 and 2009, respectively. She is currently working toward the Ph.D. degree in the Department of Electrical and Computer Engineering, Florida International University (FIU), Miami, FL, USA.

She is a Research Assistant in ElectroMagnetic Laboratory, FIU. Her research interests include the optimal design of strongly couple magnetic resonant (SCMR) systems for wireless power transfer (WPT), novel broadband and multiband WPT system design using conformal SCMR method, and miniaturized SCMR systems in the various applications such as sensors, implantable biomedical devices, and modern communication devices.

Ms. Hu received the FIU Dissertation Year Fellowship Award in 2016. She is a member of the IEEE Antennas and Propagation Society, the IEEE Industrial Electronics Society, and the IEEE Power Electronics Society.

Stavros V. Georgakopoulos (S'93–M'02–SM'11) received the Diploma from the University of Patras, Patras, Greece, in June 1996, and the M.S. and Ph.D. degrees from Arizona State University, Tempe, FL, USA, in 1998, and 2001, respectively, all in electrical engineering.

From 2001 to 2007, he was a Principal Engineer at SV Microwave, Inc. Since 2007, he has been with the Department of Electrical and Computer Engineering, Florida International University (FIU), Miami, FL, where he is currently an Associate Professor. His current research interests include wireless powering of portable, wearable, and implantable devices, novel antennas, and wireless sensors.

Dr. Georgakopoulos received the 2015 FIU President's Council Worlds Ahead Faculty Award, which is the highest honor FIU extends to a faculty member for excelling in research, teaching, mentorship, and service. He has been serving as an Associate Editor of the IEEE TRANSACTIONS ON ANTENNAS AND PROPAGATION since 2013.